JACS
JOURNAL OF THE AMERICAN CHEMICAL SOCIETY
Article
pubs.acs.org/JACS

Semiconducting Single Crystals Comprising Segregated Arrays of Complexes of C_{60}

Jonathan C. Barnes,[†,§] Edward J. Dale,[†] Aleksandrs Prokofjevs,[†] Ashwin Narayanan,[‡] Ian C. Gibbs-Hall,[†] Michal Juríček,[†,∥] Charlotte L. Stern,[†] Amy A. Sarjeant,[†] Youssry Y. Botros,[⊥,#] Samuel I. Stupp,[†,‡,∇] and J. Fraser Stoddart*[,†]

[†]Departments of Chemistry and [‡]Materials Science and Engineering, Northwestern University, 2145 Sheridan Road, Evanston, Illinois 60208, United States

[§]Department of Chemistry, Massachusetts Institute of Technology, 77 Massachusetts Avenue, Cambridge, Massachusetts 02139 United States

[∥]Department of Chemistry, University of Basel, St. Johanns-Ring 19, 4056 Basel, Switzerland

[⊥]University Research Office, Intel Corporation, Building RNB-6-61, 2200 Mission College Boulevard, Santa Clara, California 95054-1549, United States

[#]Joint Center of Excellence in Integrated Nano-Systems (JCIN), King Abdul-Aziz City for Science and Technology (KACST), P.O. Box 6086, Riyadh 11442, Kingdom of Saudi Arabia

[∇]Simpson Querrey Institute for BioNanotechnology, 303 East Superior Street, 11th Floor, Chicago, Illinois 60611, United States

Supporting Information

ABSTRACT: Although pristine C_{60} prefers to adopt a face-centered cubic packing arrangement in the solid state, it has been demonstrated that noncovalent-bonding interactions with a variety of molecular receptors lead to the complexation of C_{60} molecules, albeit usually with little or no control over their long-range order. Herein, an extended viologen-based cyclophane—$ExBox_2^{4+}$—has been employed as a molecular receptor which, not only binds C_{60} one-on-one, but also results in the columnar self-assembly of the 1:1 inclusion complexes under ambient conditions. These one-dimensional arrays of fullerenes stack along the long axis of needle-like single crystals as a consequence of multiple noncovalent-bonding interactions between each of the inclusion complexes. The electrical conductivity of these crystals is on the order of 10^{-7} S cm^{-1}, even without any evacuation of oxygen, and matches the conductivity of high-quality, unfunctionalized C_{60}-based materials that typically require stringent high-temperature vaporization techniques, along with the careful removal of oxygen and moisture, prior to measuring their conductance.

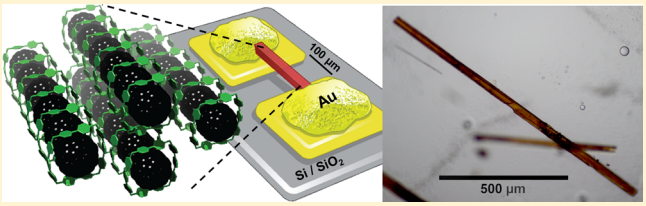

1. INTRODUCTION

Since the early discoveries[1] of C_{60}, research on fullerenes has blossomed[2] rapidly, and considerable effort has been expended with a view to understanding and exploiting the band structure[3] of doped[4] and undoped[2] fullerenes in order to capitalize on their electronic properties in devices such as organic field-effect transistors[5] (OFETs) and organic photovoltaic (OPV) solar cells.[6] Host−guest[7] chemistry has been employed in an effort to introduce solution-based techniques for the isolation and processing of C_{60}. Some of the objectives of this work have been to obtain pure fullerenes on a large scale[8a,11g] and to control the packing arrangement of one C_{60} molecule with respect to others on surfaces.[9] The more commonly used hosts, such as calixarenes,[8] γ-cyclodextrin,[10] porphyrin-based cyclic dimers,[11] cyclotriveratrylenes,[12] and cycloparaphenylenes,[13] have all been shown to bind C_{60}, usually through enthalpy-driven mechanisms,[14] such as donor−acceptor interactions where the host is the donor and C_{60} is the acceptor. Although these hosts bind C_{60} with high affinities—K_a values typically on the order of 10^5−10^8 M^{-1} in toluene—their 1:1 or 2:1 complexes typically result in either the complete isolation of the fullerenes or the clustering of only a handful of fullerene molecules in the crystalline lattice. This isolated arrangement of C_{60} molecules is not ideally suited to electronic applications where the ability to move electrons between them in a bulk material is important for the performance of devices such as OFETs. There are, however, some instances where multiple C_{60} molecules have been positioned within close contact of each other, resulting[15] in their incorporation into stable one-dimensional arrays. The most notable example of this kind of intermolecular arrangement was discovered by Luzzi et al.,[16] who observed several C_{60} molecules residing within the cavities of single-walled carbon nanotubes (SWCNTs) so as to form a

Received: December 20, 2014
Published: January 12, 2015

DOI: 10.1021/ja512959g
J. Am. Chem. Soc. 2015, 137, 2392−2399

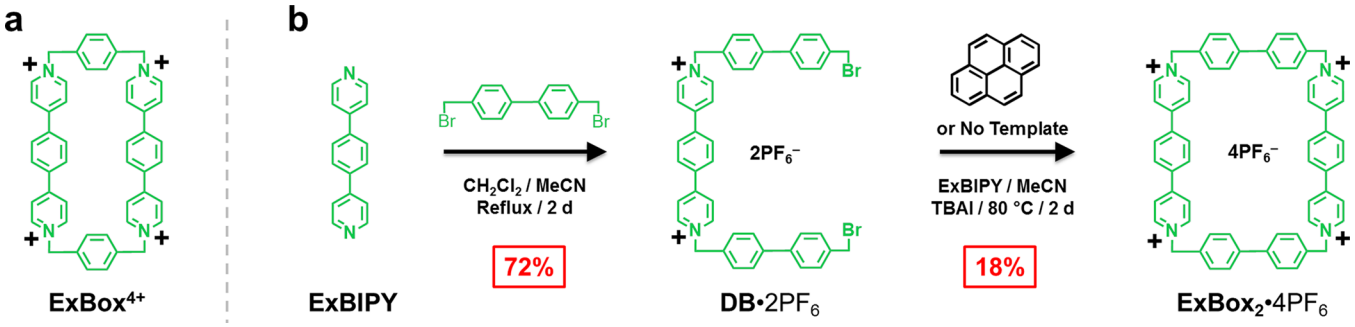

Figure 1. (a) Structural formula of **ExBox**$^{4+}$. (b) Synthesis of **ExBox**$_2$·4PF$_6$ from its precursors, **ExBIPY** and **DB**·2PF$_6$.

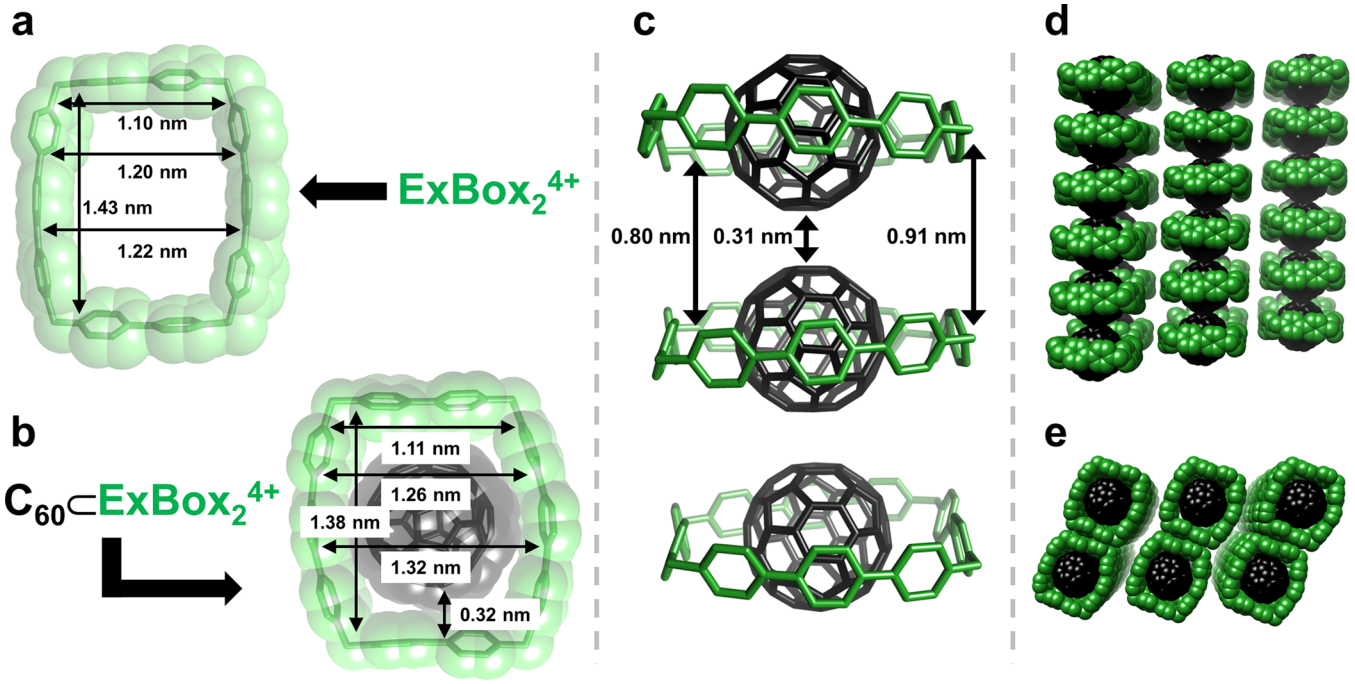

Figure 2. (Super)structures of (a) **ExBox**$_2^{4+}$ and (b) C_{60}⊂**ExBox**$_2^{4+}$ obtained from X-ray diffraction analyses performed on their respective single crystals. The close packing arrangement of each C_{60}⊂**ExBox**$_2^{4+}$ results in (c) a fullerene-to-fullerene distance of 0.31 nm (atom-to-atom) between the aligned C_{60} molecules. The side-on view (d) and plan view (e) of the solid-state superstructure illustrate the close packing arrangement of each inclusion complex into segregated one-dimensional arrays that propagate the whole length of the crystal.

supramolecular assembly that has been referred[16] to as a "nano-peapod", despite the fact that only 5% of the SWCNTs are occupied. Although the ability to incorporate C_{60} molecules into the cavities of SWCNTs has been raised[17] to 80−85% more recently, it seems that full occupancy will be difficult to achieve. In addition to the challenge of obtaining complete alignment of the host SWCNTs throughout the bulk material, the role of C_{60} in these nano-peapods is to enhance the existing semiconducting properties[18] of the SWCNTs through a charge-transfer mechanism[19] with the electron-deficient fullerene. Similarly, the nanostructure and electrical performance of fullerene−polymer blends that have been reported[20] previously are dictated more so by the side chains and semiconducting properties of the electron-rich component, respectively, than by the C_{60} molecules themselves.

We have reported previously on a family of box-like cyclophanes,[21] the so-called **ExBox**$^{4+}$ series of tetracationic extended bipyridinium-based receptors which possess the ability to bind polycyclic aromatic hydrocarbons (PAHs), ranging in size from two through seven fused benzenoid rings. The binding of PAHs inside the cavities of these cyclophanes is enthalpically driven, usually as a consequence of the π-electron-rich PAHs entering into strong donor−acceptor interactions with the π-electron-deficient **ExBox**$^{4+}$ series. Recently, we have synthesized (Figure 1) a new member of the **ExBox**$^{4+}$ family wherein each *p*-xylylene bridge has been expanded by one paraphenylene ring, increasing the width of the cavity relative to that (Figure 1a) of the original **ExBox**$^{4+}$. This structural modification results in the near doubling of the width of the cavity from 0.69 to 1.22 nm at the longest atom-to-atom distance. Since this novel tetracationic cyclophane is approximately twice the width of the original **ExBox**$^{4+}$, we use the descriptor **ExBox**$_2^{4+}$. Herein, we demonstrate that this π-electron-deficient host possesses a cavity of a size suitable for binding the electron-deficient fullerene, C_{60}, predominantly as a consequence of solvophobic processes in solution that result (Figure 2) in the self-assembly of the C_{60}⊂**ExBox**$_2^{4+}$ 1:1 inclusion complexes into continuous one-dimensional arrays which span the length of the millimeter-sized crystals. The room-temperature dark electrical conductivity of these crystals under ambient conditions surpasses, by several orders of magnitude, that reported[22] for undoped, pure C_{60}-based

DOI: 10.1021/ja512959g
J. Am. Chem. Soc. 2015, 137, 2392−2399

materials where O_2 was not evacuated. The values obtained also match the electrical conductivity of crystals and films comprised of C_{60} which are normally prepared through stringent sublimation/vapor transport techniques,[23] followed by the exhaustive removal of O_2. Moreover, we describe how $\mathbf{ExBox_2}^{4+}$ also serves as a suitable host for the radical anion $C_{60}^{\bullet-}$ on account of favorable electrostatic interactions between the tetracationic host and the anionic fullerene.

2. EXPERIMENTAL SECTION

The full experimental details are provided in the Supporting Information (SI). Below, the most important information is briefly summarized.

Synthesis of $\mathbf{ExBox_2}\cdot 4PF_6$. A mixture of **ExBIPY** (66.8 mg, 288 μmol), **DB**·$2PF_6$ (300 mg, 288 μmol), and TBAI (21.0 mg, 58.0 μmol) in dry MeCN (96 mL) was stirred at 80 °C for 48 h. Concentrated HCl was added to halt the reaction and to precipitate the crude product from the MeCN solution. The precipitate was collected by filtration and washed (Me_2CO and CH_2Cl_2) in order to remove the residual tetrabutylammonium salt. The crude product was dissolved in H_2O, precipitated as its PF_6^- salt by adding solid NH_4PF_6, and collected by filtration. It was then subjected to column chromatography (SiO_2:MeCN and 0.05−0.25% NH_4PF_6 in MeCN), followed by reverse-phase HPLC using a binary solvent system (MeCN and H_2O with 0.1% CF_3CO_2H). After removal of MeCN, pure $\mathbf{ExBox_2}\cdot 4PF_6$ (72.8 mg, 18%) was obtained as a white solid after precipitation with NH_4PF_6. HRMS-ESI for $\mathbf{ExBox_2}\cdot 4PF_6$: calcd for $C_{60}H_{48}F_{24}N_4P_4$, m/z = 1259.2804 $[M - PF_6]^+$; found 1259.2735 $[M - PF_6]^+$. ^{1}H NMR (500 MHz, CD_3CN, ppm): δ_H 8.82 (H_α, d, J = 7.0 Hz, 8H), 8.24 (H_β, d, J = 7.0 Hz, 8H), 8.01 (H_γ, s, 8H), 7.68 (H_{Phen}, d, J = 8.4 Hz, 8H), 7.55 (H_{Phen}, d, J = 8.4 Hz, 8H), 5.74 (H_{CH_2}, s, 8H). ^{13}C NMR (125 MHz, CD_3CN, ppm): δ_C 155.8, 145.3, 141.5, 137.7, 134.9, 130.5, 130.2, 128.7, 126.8, 64.7.

X-ray Diffraction. *Crystal Parameters of* $\mathbf{ExBox_2}\cdot 4PF_6$. $[C_{60}H_{48}N_4\cdot(PF_6)_4]\cdot(CH_3CN)_8$, colorless blocks (0.35 × 0.35 × 0.05 mm), monoclinic, $P2_1/n$; a = 16.2695(7), b = 15.9492(7), and c = 16.5922(7) Å; α = 90.000, β = 110.464(3), and γ = 90.000°; V = 4033.7(3) Å^3, Z = 2, T = 99.99 K, ρ_{calc} = 1.427 g cm^{-3}, μ = 1.806 mm^{-1}. Data were collected at 100 K on a Bruker Kappa APEX2 CCD diffractometer equipped with a Cu Kα microsource with Quazar optics. Of a total of 21 617 reflections that were collected, 6605 were unique. Final R_1 = 0.0790 and wR_2 = 0.2104. Distance restraints were imposed on the disordered PF_6^- anions and MeCN molecules. Rigid-bond restraints were also imposed on the displacement parameters as well as restraints on similar amplitudes separated by less than 1.7 Å on the disordered molecules. Deposited as CCDC No. 1022763.

Crystal Parameters of $C_{60}\subset\mathbf{ExBox_2}\cdot 4PF_6$. $C_{60}\subset C_{60}H_{48}N_4\cdot(PF_6)_4\cdot((CH_3)_2NCHO)_2\cdot(C_6H_5CH_3)_6$, red blocks (0.45 × 0.10 × 0.06 mm), triclinic, $P\bar{1}$; a = 17.5692(4), b = 19.4448(5), and c = 20.6000(5) Å; α = 83.1741(17), β = 65.6972(15), and γ = 82.9265(16)°; V = 6347.0(3) Å^3, Z = 2, T = 99.94 K, ρ_{calc} = 1.478 g cm^{-3}, μ = 1.396 mm^{-1}. Data were collected at 100 K on a Bruker Kappa APEX2 CCD diffractometer equipped with a Cu Kα microsource with MX optics. Of a total of 43 241 reflections that were collected, 20 638 were unique. Final R_1 = 0.1091 and wR_2 = 0.2692. The enhanced rigid-bond restraint was applied globally. Group anisotropic displacement parameters were refined for the disordered toluene solvents. Deposited as CCDC No. 1022765.

Computational Protocol. All calculations were performed using the GAMESS US (Rev. 1, May 2013) suite of computational programs. Geometries were optimized in the gas phase using the hybrid PBE-GGA functional (DFTTYP=PBE) modified with Grimme's empirical dispersion correction (2010 implementation) including the $E^{(3)}$ nonadditive energy term. The basis set used for geometry optimization was def2-SVP, as obtained from LANL Basis Set Exchange Web site. All structures were confirmed to be true energy minima on the potential energy surfaces by performing frequency analysis. The geometry of C_{60} during optimization was constrained to T_h symmetry (the more appropriate I_h point group is not available in GAMESS US). Starting geometries of $\mathbf{ExBox_2}^{4+}$ and $C_{60}\subset\mathbf{ExBox_2}^{4+}$ were obtained from the corresponding solid-state (super)structures and by means of initial semiempirical calculations, with the C_{2h} point group being chosen for both (super)structures. The optimized geometry of the $C_{60}\subset\mathbf{ExBox_2}^{4+}$ complex predicts all major features of the solid-state superstructure. See SI for references related to this computational investigation.

Cyclic Voltammetry. CV experiments were carried out at room temperature in argon-purged solutions in 1:1 DMF/PhMe with a Gamry multipurpose instrument (Reference 600) interfaced to a personal computer. All CV experiments were performed using a glassy carbon working electrode (0.071 cm^2). The electrode surface was polished routinely with a 0.05 μm alumina−water slurry on a felt surface immediately before use. The counter electrode was a Pt coil, and the reference electrode was a Ag/AgCl electrode. The concentration of the supporting electrolyte, tetrabutylammonium hexafluorophosphate ($TBAPF_6$), was 0.10 M. The CV cell was dried in an oven immediately before use, and argon was flushed continually through the cell as it was cooled to room temperature to avoid condensation of water.

Optical Absorption Spectroscopy. UV−vis absorbance spectra were recorded using a UV-3600 Shimadzu spectrophotometer. The path length of the cuvette in all cases was 2 mm. For the spectroelectrochemical (SEC) measurements, a platinum mesh was used as the working electrode, a platinum coil functioned as the counter electrode, and the reference was a Ag/AgCl electrode. The solvent consisted of a 1:1 DMF/PhMe solution of 0.1 M $TBAPF_6$ electrolyte. The applied voltage was controlled by a Gamry Multipurpose instrument (Reference 600) interfaced to a PC while absorption scans were obtained.

Isothermal Titration Calorimetry. ITC Experiments were performed on a MicroCal system, VP-ITC model. A DMF/PhMe solution of C_{60} was employed as the guest solution in a 1.8 mL cell. A solution of $\mathbf{ExBox_2}\cdot 4PF_6$ (in DMF/PhMe), used as the host, was added by injecting 10 μL of titrant (30×) over 20 s with a 240 s interval between injections. Thermodynamic information was calculated employing a one-site binding model utilizing data from which the heat of dilution of the guest was subtracted, with the average of three runs being reported.

Conductivity Measurements. Crystals of the 1:1 inclusion complex were obtained by dissolving $\mathbf{ExBox_2}\cdot 4PF_6$ (∼10 mg) in DMF (2 mL) in a 20 mL scintillation vial. A saturated C_{60} solution in PhMe was added to the point where the mixture appeared slightly opaque. After a single drop of DMF had been added, the solution became transparent once again, and the vial was placed in a jar containing iPr$_2$O (∼20 mL). Slow vapor diffusion of iPr$_2$O into the resulting DMF/PhMe solution over a period of 3−4 d yielded red single crystals of $C_{60}\subset\mathbf{ExBox_2}\cdot 4PF_6$. The presence of the 1:1 inclusion complex was confirmed by unit cell measurements using X-ray diffraction. The crystals were washed with a dilute solution of DMF in PhMe and stored in hexanes prior to conductivity measurements.

Four-inch Silicon Quest International Si wafers with a 300 nm oxide surface coating were used as substrates on which electrodes were fabricated. The wafers were cut into 2 × 2 cm squares using a diamond cutter, scrubbed with soapy water, cleaned by ultrasonication in a 1:1:1 mixture of Me_2CO/MeOH/iPrOH, and then blown dry in a stream of N_2 gas. Electrodes (spaced at 100 μm) were patterned onto the surface of the wafer by thermally evaporating 6 Å of Cr and then 50 nm of Au through a defined shadow mask at a pressure of 10^{-6} mbar. Single crystals of $C_{60}\subset\mathbf{ExBox_2}\cdot 4PF_6$ were picked up using a Pelco vacuum pick-up system and placed across the electrodes. The ends of the crystals were painted with Pelco conductive gold paste to secure a conducting pathway to the patterned electrodes.

Two-probe measurements were performed at a Signatone probe station, in conjunction with an Agilent 4155C semiconductor parameter analyzer. Current output was measured at room temperature for DC voltage sweeps from 0 to +1 V. All measurements were carried out in a US FED STD 209E Class 100 (ISO 5) clean room.

DOI: 10.1021/ja512959g
J. Am. Chem. Soc. 2015, 137, 2392−2399

3. RESULTS AND DISCUSSION

The synthesis (Figure 1b) of **ExBox$_2$**·4PF$_6$ follows a modified procedure[21c] that makes use of tetrabutylammonium iodide (TBAI) as a catalyst during the reaction of **ExBIPY** with **DB**·2PF$_6$. Using this procedure, we were able to obtain several hundred milligrams of **ExBox$_2$**·4PF$_6$ in 18% yield, allowing solution-phase and solid-state investigations to be carried out in the presence of C$_{60}$. See the SI for a detailed synthetic protocol and ^{1}H and ^{13}C NMR spectroscopic and high-resolution mass spectrometric characterization of **ExBox$_2$**·4PF$_6$.

The solid-state structure (Figure 2a) illustrates the size of the cavity of **ExBox$_2^{4+}$**, where its atom-to-atom dimensions measure 1.43 nm in length and 1.22 nm at its widest point. The ∼1.75 nm^2 cavity is capable of ensconcing two guests, as evidenced by its ability to bind either two solvent or two planar perylene molecules (see solid-state superstructures in the SI, Figure S4). Moreover, the superstructure (Figure S1) of **ExBox$_2^{4+}$** illustrates how crystal packing forces dictate a herringbone packing arrangement when no guest is present, where each cyclophane is staggered relative to one another. In contrast, the solid-state superstructure of the 1:1 inclusion complex C$_{60}$⊂**ExBox$_2^{4+}$** (Figure 2b) highlights the dimensions, where, atom-to-atom, it measures 1.38 nm in length and 1.32 nm at its widest point. This change in geometry of the host in the 1:1 complex relative to that of the empty host suggests that **ExBox$_2^{4+}$** is willing to contort and twist its original conformation in order to shorten its length and increase its width such that it can embrace C$_{60}$ in an approximately centrosymmetric fashion. Figure 2c portrays the intercomplex atom-to-atom distances where the encircled C$_{60}$ molecules are separated by 0.31 nm. This distance is indicative of van der Waals interactions between the fullerenes of adjacent inclusion complexes. The side-on view (Figure 2d) of the C$_{60}$⊂**ExBox$_2^{4+}$** solid-state superstructure illustrates the complete alignment of the inclusion complexes into discrete one-dimensional arrays. Moreover, the plan view (Figure 2e) of these discrete linear arrays shows how each C$_{60}$ molecule in each self-assembled supramolecular wire[24]—i.e., each stack of 1:1 inclusion complexes—is segregated from the others as a consequence of intermolecular biphenylene π−π stacking and ExBIPY^{2+} subunit slipped alignments between adjacent hosts. This arrangement contrasts with the typical fcc packing of pure C$_{60}$ at room temperature and ultimately leads to van der Waals interactions between fullerenes propagated in one dimension throughout the crystal lattice.

In order to understand the nature of molecular recognition that occurs in solution, which ultimately results in the self-assembly of the C$_{60}$⊂**ExBox$_2^{4+}$** in the solid state, we carried out (i) UV−vis absorption spectroscopy, (ii) isothermal titration calorimetry (ITC), and (iii) density functional theory (DFT) calculations. To elucidate the binding affinity between C$_{60}$ and **ExBox$_2^{4+}$** in solution, a UV−vis titration was performed (Figure S8) in a DMF/PhMe mixture. After a 2:1 ratio of **ExBox$_2$**·4PF$_6$:C$_{60}$ had been achieved, the change in the absorbance of the complex at 450 nm was plotted against the change in **ExBox$_2$**·4PF$_6$ concentration, and a nonlinear least-squares analysis was applied, resulting in a calculated association constant (K_a) of (7.1 ± 2.7) × 10^3 M^{-1}.

ITC was carried out (Figure S10) in a 1:1 mixture of DMF/PhMe at 298 K in order to gain additional insight into the binding thermodynamics in solution. The results from this ITC investigation indicate that the binding of C$_{60}$ by **ExBox$_2^{4+}$** in solution is a favorable process that is predominantly driven by entropy, as evidenced by ΔH = 2.6 ± 0.3 kcal mol^{-1} and ΔS = 23.9 ± 0.5 cal mol^{-1} K^{-1}, with an overall ΔG = −4.6 ± 0.3 kcal mol^{-1}. Importantly, the K_a value ((2.5 ± 1.3) × 10^3 M^{-1}) obtained from ITC is in good agreement with that ((7.1 ± 2.7) × 10^3 M^{-1}) obtained from the UV−vis titration. The fact that this K_a value is lower than that for traditional electron-rich C$_{60}$ hosts is not surprising, given the unfavorable enthalpic interactions between the π-electron-poor **ExBox$_2^{4+}$** and C$_{60}$.

DFT calculations were performed (Figure 3) through gas-phase geometry optimization of the solid-state superstructure in order to determine the orbital interactions of the host and guest molecules within C$_{60}$⊂**ExBox$_2^{4+}$**. These calculations support the experimental observations in terms of the host's ability to contort and twist its ground-state conformation in order to accommodate (Figure 3a−c) C$_{60}$ in an almost centrosymmetric fashion. Furthermore, the theoretical calculations indicate (Figure 3d) that the HOMO of the complex resides primarily on the C$_{60}$ molecule, while the LUMO is centered on the ExBIPY^{2+} subunit. This assignment of the frontier molecular orbitals is contrary to typical donor−acceptor systems involving C$_{60}$, where the latter usually functions as the acceptor. Additionally, the lowest lying unoccupied molecular orbital centered (Figure 3d) on C$_{60}$ is LUMO+2, while the highest lying occupied orbital of the host, primarily composed of the biphenylene subunit, is HOMO−5. These van der Waals interactions between host and guest, in combination with those between the hosts of adjacent inclusion complexes (i.e., biphenylene π−π stacking and ExBIPY^{2+} slipped stacking, as well as ion−dipole interactions) in the solid-state superstructure, undoubtedly play a role in the self-assembly process.

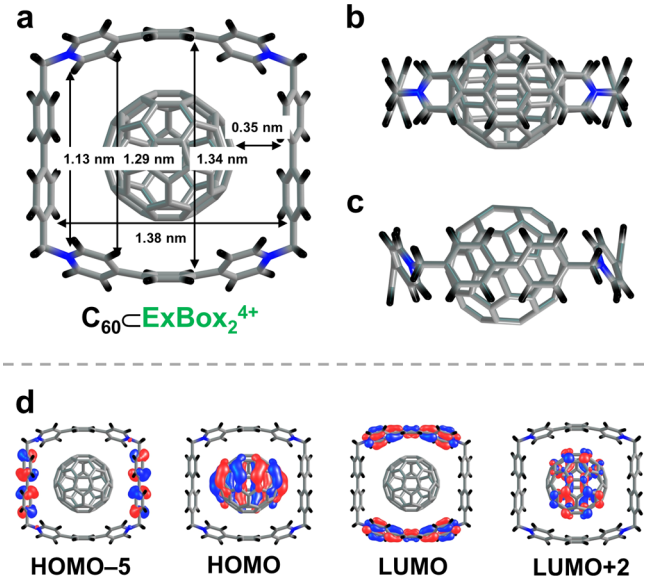

Figure 3. DFT-optimized geometry of the 1:1 inclusion complex, resulting in (a) a superstructure similar to that obtained experimentally. Calculated geometries of the inclusion complex viewed from (b) the ExBIPY^{2+} and (c) the biphenyl side-on perspectives illustrate the centrosymmetric fashion with which C$_{60}$ is bound by **ExBox$_2^{4+}$**, in agreement with the solid-state superstructure. (d) Orbital depictions of the 1:1 inclusion complex showing that the HOMO−5 resides on the biphenyl subunits of **ExBox$_2^{4+}$**, the HOMO and LUMO +2 are centered on the bound C$_{60}$, and the LUMO resides on the two ExBIPY^{2+} subunits.

DOI: 10.1021/ja512959g
J. Am. Chem. Soc. 2015, 137, 2392−2399

To determine whether the energy gap between the HOMO and LUMO of C_{60} is affected once C_{60} is encircled by $\mathbf{ExBox_2}^{4+}$ in solution, cyclic voltammetry measurements were carried out (Figure 4) in DMF/PhMe containing 0.1 M $TBAPF_6$ (Ag/AgCl reference electrode) in order to estimate the approximate ionization potential and electron affinity energies. A general depiction of the complex formed between C_{60} and $\mathbf{ExBox_2}^{4+}$, in addition to the scenario when C_{60} is reduced to the radical anion through the addition of one electron, is illustrated in Figure 4a. The CV measurements reveal that the first and second redox waves of $\mathbf{ExBox_2}^{4+}$ (Figure 4b, green trace) are broad and overlap one another on account of the weakened electronic coupling between the individual pyridinium rings of the viologen subunits of the host. Furthermore, the first three one-electron redox processes of C_{60} are defined (Figure 4b, black trace) in the DMF/PhMe solvent mixture, as well as the redox processes (Figure 4b, red trace) for $C_{60}\subset\mathbf{ExBox_2}^{4+}$. The redox potentials for each component of the 1:1 complex undergo only minor shifts in comparison to those of the unbound C_{60} and $\mathbf{ExBox_2}^{4+}$ molecules. The most notable change is observed (Table 1) for the first one-electron reduction of C_{60}, where the peak reduction potential shifts by +30 mV (−0.34 to −0.31 V) when C_{60} is complexed with $\mathbf{ExBox_2}^{4+}$. This small shift changes the energy of the C_{60} LUMO from −4.06 to −4.09 eV, where the reduction potential ($E'_{red,bound}$ = −0.34 V) was used in the equation[25] $E_{LUMO,bound}$ = ($E'_{red,bound}$ + 4.4)·eV to estimate the C_{60} LUMO energy level when C_{60} is encircled by $\mathbf{ExBox_2}^{4+}$. The energy levels of the HOMO for the bound and unbound C_{60} were calculated in a similar manner using the peak (both +1.12 V) oxidation potentials in the equation E_{HOMO} = (E'_{ox} + 4.4)·eV. From the peak oxidation potentials, this calculation yields E_{HOMO} = −5.52 eV for both the bound and unbound states of C_{60}. Calculating the differences between the HOMO/LUMO energy values from the peak potentials of bound and unbound C_{60} (Table 1) results in energy gaps (E_g) of $E_{g,bound}$ = 1.43 eV and $E_{g,unbound}$ = 1.46 eV. Doing similar calculations except using the onset potentials (Figure S9), $E_{g,bound,onset}$ = 1.11 eV and $E_{g,unbound,onset}$ = 1.09 eV. These orbital energy calculations show that $\mathbf{ExBox_2}^{4+}$ has little effect on the energy gap of C_{60} during the formation of the $C_{60}\subset\mathbf{ExBox_2}^{4+}$ inclusion complex in solution.

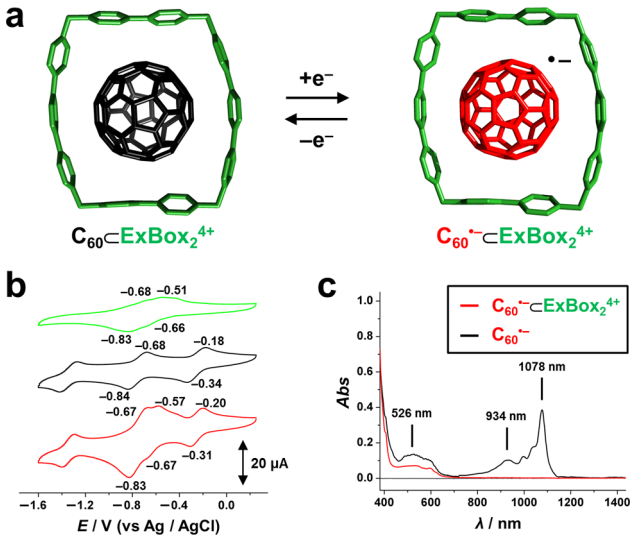

Figure 4. (a) Generation of the reduced inclusion complex $C_{60}^{\bullet-}\subset\mathbf{ExBox_2}^{4+}$ after the addition of one electron to C_{60}. (b) When cyclic voltammetry of $\mathbf{ExBox_2}^{4+}$ (green trace), C_{60} (black trace), and $C_{60}\subset\mathbf{ExBox_2}^{4+}$ (red trace) was carried out, a shift of only +30 mV was observed for the first reduction wave of the bound C_{60} in a DMF/PhMe solvent system and 0.1 M $TBAPF_6$ electrolyte. (c) Spectroelectrochemistry performed in a 2 mm cell on the bound C_{60} (black trace) at an applied potential of −0.49 V produced the signature radical absorption peaks for $C_{60}^{\bullet-}$ at 934 and 1078 nm. In the presence of an equimolar amount of $\mathbf{ExBox_2}^{4+}$ (red trace), these radical absorption peaks were nonexistent, indicating strong ion-pairing between the host and reduced guest.

Since the first reduction wave of C_{60} does not overlap with the first reduction wave of $\mathbf{ExBox_2}^{4+}$, it is possible to carry out a SEC analysis (Figure 4c) of the $C_{60}^{\bullet-}\subset\mathbf{ExBox_2}^{4+}$ inclusion complex where the radical anion of C_{60} (namely, $C_{60}^{\bullet-}$) can be generated electrochemically by applying a potential of −0.49 V to a 0.42 mM DMF/PhMe solution of the complex for ∼30 min. The radical absorption bands of $C_{60}^{\bullet-}$ (Figure 4c, black trace) appear at 934 and 1078 nm and correspond to the allowed transition[26] of the unpaired electron from the singly occupied molecular orbital (SOMO) to the nearest unoccupied molecular orbital, $t_{1u} \rightarrow t_{1g}$. In the presence of an equimolar amount of $\mathbf{ExBox_2}^{4+}$, however, the signature radical absorption bands for $C_{60}^{\bullet-}$ are nonexistent. The absence of these diagnostic radical absorption bands is consistent with previously reported[27] solvated ion-pairing interactions in systems containing $C_{60}^{\bullet-}$.

In order to measure the bulk electrical conductivity of the $C_{60}\subset\mathbf{ExBox_2}^{4+}$ inclusion complexes, single crystals (Figure 5a) of the 1:1 complex were grown using a modified procedure (see SI). These crystals were never placed under vacuum to remove residual O_2, and conductivity measurements were carried out under ambient conditions. Crystallographic indexing proved (Figure 5b) that the fullerene arrays were aligned with the long axis of the crystal. In order to construct a device (Figure 5c), single crystals of $C_{60}\subset\mathbf{ExBox_2}\cdot 4PF_6$ were placed across gold electrodes spaced 100 μm apart on a Si/SiO_2 wafer. The ends of the crystal were painted with a conductive gold paste to secure a conducting pathway to the patterned electrodes.

Table 1. Peak and Onset Redox Potentials of Bound and Unbound C_{60} (vs Ag/AgCl) in DMF/PhMe and the Corresponding Orbital Energy Levels

	redox potentials				orbital energy levels[a]								
	peak (V)[b]		onset (V)[c]		peak (eV)[b]				onset (eV)[c]				
	E'_{red}	E'_{ox}	E'_{red}	E'_{ox}	E_{LUMO}	−	E_{HOMO}	=	E_g	E_{LUMO}	−	E_{HOMO}	=	E_g
$C_{60}\subset\mathbf{ExBox_2}^{4+}$	−0.31	+1.12	−0.19	+0.90	−4.09	−	(−5.52)	=	1.43	−4.21	−	(−5.30)	=	1.09
C_{60}	−0.34	+1.12	−0.19	+0.92	−4.06	−	(−5.52)	=	1.46	−4.21	−	(−5.32)	=	1.11

[a]Calculated from the equation $E_{LUMO/HOMO}$ = (E'_{redox} + 4.4)·eV. [b]Determined from the plateau/middle of the redox wave. [c]Determined from the intersection of the lines that are tangent to the baseline before the redox wave and to the rise of the redox wave itself (see SI)

DOI: 10.1021/ja512959g
J. Am. Chem. Soc. 2015, 137, 2392−2399

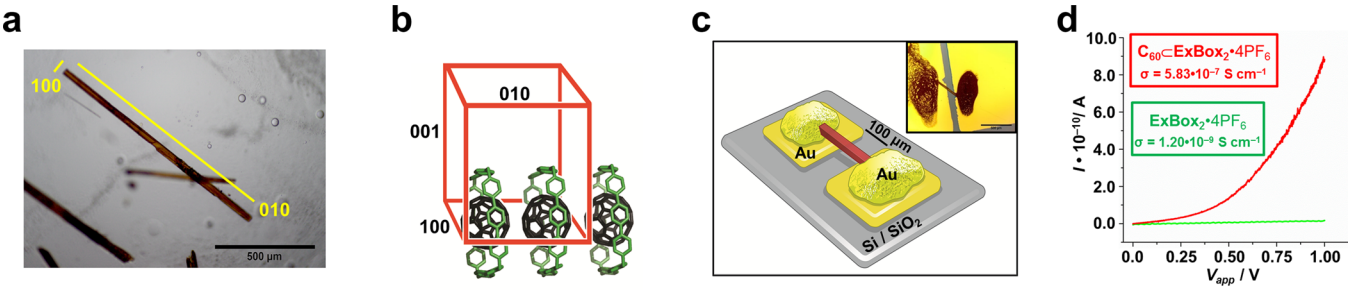

Figure 5. (a) Single crystals of C_{60}⊂**ExBox**$_2$·4PF_6 were grown by slow vapor diffusion of iPr$_2$O into a DMF/PhMe solution and were indexed to confirm (b) the orientation of the C_{60} molecules before the crystal was mounted (c) onto a Si/SiO_2 wafer patterned with gold electrodes, followed by the application of a gold paste to the ends of the crystal. The scale bar for the inset device picture is 500 μm. (d) Electrical conductivity measurements performed on single crystals of C_{60}⊂**ExBox**$_2$·4PF_6 and **ExBox**$_2$·4PF_6 revealed a difference of nearly 2.5 orders of magnitude in conductivity when C_{60} is present.

Dark electrical current was measured (Figure 5d, red trace) at room temperature between 0 and +1 V. Conductivity was extrapolated within the strict ohmic region (0 to +0.15 V) of the measured I−V curve, since the region beyond +0.15 V is more representative of a Shottky barrier. Multiple single crystals were analyzed using this method, and the average electrical conductivity was found to be $(5.83 \pm 0.15) \times 10^{-7}$ S cm^{-1}. This value is nearly 2−3 orders of magnitude greater than the first reported electrical conductivity of pure C_{60} single crystals[22a,b] and films[22b−e] where O_2 was not removed. While no effort was made to remove O_2 from the C_{60}⊂**ExBox**$_2$·4PF_6 crystals, the room-temperature dark electrical conductivity is still comparable to that[23] (10^{-6}−10^{-8} S cm^{-1}) measured in pure C_{60}-based materials where the strict removal of O_2 contamination was required. Unlike the stringent high-temperature vaporization techniques for the preparation of these purely C_{60}-based materials, the preparation of C_{60}⊂**ExBox**$_2$·4PF_6 crystals relies on facile, room-temperature crystallization from solution. In the absence of C_{60}, control measurements (Figure 5c, green trace) on **ExBox**$_2$·4PF_6 single crystals resulted in an average conductivity of $(1.20 \pm 0.17) \times 10^{-9}$ S cm^{-1}. Based on these measurements, the necessity of C_{60} for higher electrical conductivities is evident, and the alignment of C_{60} molecules into discrete supramolecular one-dimensional arrays leads to improved electrical conductivity over **ExBox**$_2^{4+}$ and C_{60} systems without the rigorous exclusion of O_2.

4. CONCLUSIONS

The semiconducting properties of C_{60} and its derivatives make them attractive components for organic molecular electronic devices, such as in OFETs and OPV solar cells. Although materials comprised of pure, undoped C_{60} have shown promise in terms of their electrical conductivity, stringent high-temperature mass transport/sublimation techniques are required to grow the single crystals and polycrystalline films. Moreover, the electrical performance of these purely C_{60}-based devices relies heavily on post-synthetic annealing techniques to remove interstitial O_2 as a consequence of their porous structure. The use of host−guest chemistry to bind C_{60} and disrupt its standard fcc packing arrangement has been achieved on a number of occasions[8−13] over the past 20 years. Although there are many examples[5,20] in the literature of one-dimensional alignment of functionalized C_{60} molecules, there are only a handful of examples[15−17] where a host has been capable of directing the formation of unfunctionalized C_{60} into discrete, one-dimensional arrays that span the entire length of millimeter-sized crystals. The C_{60}⊂**ExBox**$_2$·4PF_6 single crystals described in this investigation are grown under ambient conditions using a solution-processable protocol that excludes O_2 during the favorable self-assembly process, leading to a situation where the removal of residual O_2 does not affect the electrical conductivity of the material, measuring $(5.83 \pm 0.15) \times 10^{-7}$ S cm^{-1}. The result of this form of crystal engineering is a conductivity value that is 2−3 orders of magnitude greater than that of the earliest reported[22] materials comprised of undoped C_{60} and matches that[23] of high-quality, nearly oxygen-free C_{60} single crystals prepared through stringent high-temperature mass transport/annealing techniques. Moreover, the tetracationic **ExBox**$_2^{4+}$ is a suitable host for binding the reduced states of C_{60}, demonstrated specifically for $C_{60}^{\bullet-}$ in this work. Since the entropically driven complexation of C_{60} by **ExBox**$_2^{4+}$ in a DMF/PhMe solution does not greatly affect the orbital energy gap of C_{60}, there is potential to implement its use in solution-processable protocols to fabricate organic-based electronic devices that would benefit from ordered assemblies of the semiconducting fullerene. The strategy reported here to create fullerene-based semiconducting supramolecular wires may potentially be applied toward (i) the fabrication of OFET devices consisting of ordered stacks of C_{60}⊂**ExBox**$_2^{4+}$, (ii) solid-state photoinduced polymerization of the ordered C_{60} molecules in the 1:1 inclusion complexes to generate polypseudorotaxanes, (iii) highly ordered conducting metallo-fullerene-based devices, and (iv) similar linear arrangements of segregated stacks with host molecules and other carbon allotropes,[28] such as C_{70} and C_{82}, as well as single-walled carbon nanotubes of appropriate diameter.

■ ASSOCIATED CONTENT

Ⓢ Supporting Information

Detailed synthetic procedures and characterization data (NMR and HRMS) for all compounds; crystallographic and spectroscopic characterization for **ExBox**$_2$·4PF_6 and its inclusion complexes. This material is available free of charge via the Internet at http://pubs.acs.org.

■ AUTHOR INFORMATION

Corresponding Author

*stoddart@northwestern.edu

Notes

The authors declare no competing financial interest.

DOI: 10.1021/ja512959g
J. Am. Chem. Soc. 2015, 137, 2392−2399

■ ACKNOWLEDGMENTS

This research is part (Project 34-947) of the Joint Center of Excellence in Integrated Nano-Systems (JCIN) at King Abdul-Aziz City for Science and Technology (KACST), Northwestern University (NU), and the National Science Foundation (NSF), Division of Materials Research (DMR-1006713). S.I.S. acknowledges support for A.N. and conductivity studies from the Office of Science, Office of Basic Energy Sciences, U.S. Department of Energy, under Award No. DE-FG02-00ER45810. The authors thank KACST, NU, and the NSF for their continued support of this research. J.C.B. and I.C.G.-H. are supported by a National Defense Science and Engineering Graduate Fellowship from the Department of Defense. J.C.B. and E.J.D. gratefully acknowledge support from the Ryan Fellowship and the NU International Institute for Nanotechnology (IIN). E.J.D. is supported by a Graduate Research Fellowship from the National Science Foundation. M.J. acknowledges The Netherlands Organisation for Scientific Research (NWO) and Marie Curie Cofund Action for their financial support (Rubicon Fellowship). The authors thank the NU Micro/Nano Fabrication Facility (NUFAB) for providing access to equipment for conductivity measurements, as well as T. Aytun (NU) and F. Rao (NU) for discussions and advice on electrical characterization. The authors also thank NU and the IIN for their support of the NMR instrumentation in the Integrated Molecular Structure Education and Research Center (IMSERC) characterization facility, as well as the State of Illinois for its support of the X-ray diffractometer and high-resolution mass spectrometer located in IMSERC.

■ REFERENCES

(1) (a) Kroto, H. W.; Heath, J. R.; O'Brien, S. C.; Curl, R. F.; Smalley, R. E. *Nature* **1985**, *318*, 162−163. (b) Krätschmer, W.; Lamb, L. D.; Fostiropoulos, K.; Huffman, D. R. *Nature* **1990**, *347*, 354−358.

(2) (a) David, W. I. F.; Ibberson, R. M.; Matthewman, J. C.; Prassides, K.; Dennis, T. J. S.; Hare, J. P.; Kroto, H. W.; Taylor, R.; Walton, D. R. M. *Nature* **1991**, *353*, 147−149. (b) Diederich, F.; Ettl, R.; Rubin, Y.; Whetten, R. L.; Beck, R.; Alvarez, M.; Anz, S.; Sensharma, S.; Wudl, F.; Khemani, K.; Koch, A. *Science* **1991**, *252*, 548−551. (c) Kroto, H. W.; Allaf, A. W.; Balm, S. P. *Chem. Rev.* **1991**, *91*, 1213−1235. (d) Rao, A. M.; Zhou, P.; Wang, K.-A.; Hager, G. T.; Holden, J. M.; Wang, Y.; Lee, W.-T.; Bi, X.-X.; Eklund, P. C.; Cornett, D. S.; Duncan, M. A.; Amster, I. J. *Science* **1995**, *259*, 955−957. (e) Roy, X.; Lee, C.-H.; Crowther, A. C.; Schenck, C. L.; Besara, T.; Lalancette, R. A.; Siegrist, T.; Stephens, P. W.; Brus, L. E.; Kim, P.; Steigerwald, M. L.; Nuckolls, C. *Science* **2013**, *341*, 157−160. (f) Dunk, P. W.; Mulet-Gas, M.; Nakanishi, Y.; Kaiser, N. K.; Rodríguez-Fortea, A.; Shinohara, H.; Poblet, J. M.; Marshall, A. G.; Kroto, H. W. *Nat. Commun.* **2014**, *5*, 5844.

(3) (a) Saito, S.; Oshiyama, A. *Phys. Rev. Lett.* **1991**, *66*, 2637−2640. (b) Lof, R. W.; van Veenendaal, M. A.; Koopmans, B.; Jonkman, H. T.; Sawatzky, G. A. *Phys. Rev. Lett.* **1992**, *68*, 3924−3927.

(4) (a) Haddon, R. C.; Hebard, A. F.; Rosseinsky, M. J.; Murphy, D. W.; Duclos, S. J.; Lyons, K. B.; Miller, B.; Rosamilia, J. M.; Fleming, R. M.; Kortan, A. R.; Glarum, S. H.; Makhija, A. V.; Muller, A. J.; Eick, R. H.; Zahurak, S. M.; Tycko, R.; Dabbagh, G.; Thiel, F. A. *Nature* **1991**, *350*, 320−322. (b) Hebard, A. F.; Rosseinsky, M. J.; Haddon, R. C.; Murphy, D. W.; Glarum, S. H.; Palstra, T. T. M.; Ramirez, A. P.; Kortan, A. R. *Nature* **1991**, *350*, 600−601.

(5) (a) Chikamatsu, M.; Nagamatsu, S.; Yoshida, Y.; Kazuhiro, S.; Yase, K.; Kikuchi, K. *Appl. Phys. Lett.* **2005**, *87*, No. 203504. (b) Chu, C.-C.; Raffy, G.; Ray, D.; Guerzo, A. D.; Kauffmann, B.; Wantz, G.; Hirsch, L.; Bassani, D. M. *J. Am. Chem. Soc.* **2010**, *132*, 12717−12723. (c) Li, H.; Tee, B. C.-K.; Cha, J. J.; Cui, Y.; Chung, J. W.; Lee, S. Y.; Bao, Z. *J. Am. Chem. Soc.* **2012**, *134*, 2760−2765. (d) Zhang, J.; Tan, J.; Ma, Z.; Xu, W.; Zhao, G.; Geng, H.; Di, C.; Hu, W.; Shuai, Z.; Singh, K.; Zhu, D. *J. Am. Chem. Soc.* **2013**, *135*, 558−561.

(6) (a) Schiros, T.; Kladnik, G.; Prezzi, D.; Ferretti, A.; Olivieri, G.; Cossaro, A.; Floreano, L.; Verdini, A.; Schenck, C.; Cox, M.; Gorodetsky, A. A.; Plunkett, K.; Delongchamp, D.; Nuckolls, C.; Morgante, A.; Cvetko, D.; Kymissis, I. *Adv. Energy Mater.* **2013**, *3*, 894−902. (b) Menke, S. M.; Luhman, W. A.; Holmes, R. J. *Nat. Mater.* **2013**, *12*, 152−157.

(7) Cram, D. J.; Cram, J. M. *Container Molecules and Their Guests*; Royal Society of Chemistry: Cambridge, UK, 1994.

(8) (a) Atwood, J. L.; Koutsantonis, G. A.; Raston, C. L. *Nature* **1994**, *368*, 229−231. (b) Barbour, L. J.; Orr, G. W.; Atwood, J. L. *Chem. Commun.* **1997**, 1439−1440. (c) Atwood, J. L.; Barbour, L. J.; Nichols, P. J.; Raston, C. L.; Sandoval, C. A. *Chem.—Eur. J.* **1999**, *5*, 990−996. (d) Sun, D.; Reed, C. A. *Chem. Commun.* **2000**, 2391−2392. (e) Pan, G.-B.; Liu, J.-M.; Zhang, H.-M.; Wan, L.-J.; Zheng, Q.-Y.; Bai, C.-L. *Angew. Chem., Int. Ed.* **2003**, *42*, 2747−2751. (f) Halder, A.; Bhattacharya, S. *Spectrochim. Acta Mol. Biomol. Spectrosc.* **2012**, 335−341. (g) Davis, C. M.; Lim, J. M.; Larsen, K. R.; Kim, D. S.; Sung, Y. M.; Lyons, D. M.; Lynch, V. M.; Nielsen, K. A.; Jeppesen, J. O.; Kim, D.; Park, J. S.; Sessler, J. L. *J. Am. Chem. Soc.* **2014**, *136*, 10410−10417. (h) Hirao, T.; Tosaka, M.; Yamago, S.; Haino, T. *Chem.—Eur. J.* **2014**, *20*, 16138−16146.

(9) (a) Effing, J.; Jonas, U.; Jullien, L.; Plesnivy, T.; Ringsdorf, H.; Diederich, F.; Thilgen, C.; Weinstein, D. *Angew. Chem., Int. Ed. Engl.* **1992**, *31*, 1599−1602. (b) Pan, G.-B.; Cheng, X.-H.; Höger, S.; Freyland, W. *J. Am. Chem. Soc.* **2006**, *128*, 4218−4219. (c) Sánchez, L.; Otero, R.; Gallego, J. M.; Miranda, R.; Martín, N. *Chem. Rev.* **2009**, *109*, 2081−2091.

(10) (a) Andersson, T.; Nilsson, K.; Sundahl, M.; Westman, G.; Wennerström. *J. Chem. Soc., Chem. Commun.* **1992**, 604−606. (b) Priyadarsini, K. I.; Mohan, H.; Tyagi, A. K.; Mittal, J. P. *J. Phys. Chem.* **1994**, *98*, 4756−4759. (c) Yoshida, Z.; Takekuma, H.; Takekuma, S.; Matsubara, Y. *Angew. Chem., Int. Ed. Engl.* **1994**, *33*, 1597−1599. (d) Zhang, Y.; Liu, W.; Gao, X.; Zhao, Y.; Zheng, M.; Li, F.; Ye, D. *Tetrahedron Lett.* **2006**, *47*, 8571−8574. (e) Zhang, Y.; Ye, D.; Gao, X.; Liu, W.; Li, F. *Fullerenes, Nanotubes, Carbon Nanostruct.* **2007**, *15*, 317−330. (f) Wang, H. M.; Wenz, G. *Beilstein J. Org. Chem.* **2012**, *8*, 1644−1651. (g) Nobusawa, K.; Payra, D.; Naito, M. *Chem. Commun.* **2014**, *50*, 8339−8342.

(11) (a) Tashiro, K.; Aida, T.; Zheng, J.-Y.; Kinbara, K.; Saigo, K.; Sakamoto, S.; Yamaguchi, K. *J. Am. Chem. Soc.* **1999**, *121*, 9477−9478. (b) Kieran, A. L.; Pascu, S. I.; Jarrosson, T.; Sanders, J. K. M. *Chem. Commun.* **2005**, 1276−1278. (c) Boyd, P. W.; Reed, C. A. *Acc. Chem. Res.* **2005**, *38*, 235−242. (d) Yanagisawa, M.; Tashiro, K.; Yamasaki, M.; Aida, T. *J. Am. Chem. Soc.* **2007**, *129*, 11912−11913. (e) Nobukuni, H.; Shimazaki, Y.; Uno, H.; Naruta, Y.; Ohkubo, K.; Kojima, T.; Fukuzumi, S.; Seki, S.; Sakai, H.; Hasobe, T.; Tani, F. *Chem.—Eur. J.* **2010**, *16*, 11611−11623. (f) Nakamura, T.; Ube, H.; Miyake, R.; Shionoya, M. *J. Am. Chem. Soc.* **2013**, *135*, 18790−18793. (g) García-Simón, C.; Garcia-Borràs, M.; Gómez, L.; Parella, T.; Osuna, S.; Juanhuix, J.; Imaz, I.; Maspoch, D.; Costas, M.; Ribas, X. *Nat. Commun.* **2014**, *5*, 5557. (h) Sakaguchi, K.; Kamimura, T.; Uno, H.; Mori, S.; Ozako, S.; Nobukuni, H.; Ishida, M.; Tani, F. *J. Org. Chem.* **2014**, *79*, 2980−2992. (i) Terao, J.; Chiba, Y.; Fujihara, T.; Tsuji, Y. *Chem. Lett.* **2014**, *43*, 1374−1376.

(12) (a) Steed, J. W.; Junk, P. C.; Atwood, J. L. *J. Am. Chem. Soc.* **1994**, *116*, 10346−10347. (b) Atwood, J. L.; Barnes, M. J.; Gardiner, M. G.; Raston, C. L. *Chem. Commun.* **1996**, 1449−1450. (c) Felder, D.; Heinrich, B.; Guillon, D.; Nicoud, J.-F.; Nierengarten, J.-F. *Chem.—Eur. J.* **2000**, *6*, 3501−3507. (d) Yang, F.; Chen, Q.; Cheng, Q.-Y.; Yan, C.-G.; Han, B.-H. *J. Org. Chem.* **2012**, *77*, 971−976.

(13) (a) Kawase, T.; Tanaka, K.; Fujiwara, N.; Darabi, H. R.; Oda, M. *Angew. Chem., Int. Ed.* **2003**, *42*, 1624−1628. (b) Kawase, T.; Oda, M. *Pure Appl. Chem.* **2006**, *78*, 831−839. (c) Iwamoto, T.; Watanabe, Y.; Sadahiro, T.; Haino, T.; Yamago, S. *Angew. Chem., Int. Ed.* **2011**, *50*, 8342−8344. (d) Xia, J.; Bacon, J. W.; Jasti, R. *Chem. Sci.* **2012**, *3*, 3018−3021.

DOI: 10.1021/ja512959g
J. Am. Chem. Soc. 2015, 137, 2392−2399

(14) Diederich, F.; Gómez-López, M. *Chem. Soc. Rev.* **1999**, *28*, 263−277.
(15) Veen, E. M.; Postma, P. M.; Jonkman, H. T.; Spek, A. L.; Feringa, B. L. *Chem. Commun.* **1999**, 1709−1710.
(16) Smith, B. W.; Monthioux, M.; Luzzi, D. E. *Nature* **1998**, *396*, 323−324.
(17) Kitaura, R.; Shinohara, H. *Chem.—Asian J.* **2006**, *1*, 646−655.
(18) Vavro, J.; Llaguno, M. C.; Satishkumar, B. C.; Luzzi, D. E.; Fischer, J. E. *Appl. Phys. Lett.* **2002**, *80*, 1450−1452.
(19) Pati, R.; Senapati, L.; Ajayan, P. M.; Nayak, S. K. *J. Appl. Phys.* **2002**, *95*, 694−697.
(20) (a) Mayer, A. C.; Toney, M. F.; Scully, S. R.; Rivnay, J.; Brabec, C. J.; Scharber, M.; Koppe, M.; Heeney, M.; McCulloch, I.; McGehee, M. D. *Adv. Funct. Mater.* **2009**, *19*, 1173−1179. (b) Miller, N. C.; Cho, E.; Gysel, R.; Risko, C.; Coropceanu, V.; Miller, C. E.; Sweetnam, S.; Sellinger, A.; Heeney, M.; McCulloch, I.; Brédas, J.-L.; Toney, M. F.; McGehee, M. D. *Adv. Energy Mater.* **2012**, *2*, 1208−1217. (c) Miller, N. C.; Cho, E.; Junk, M. J. N.; Gysel, R.; Risko, C.; Kim, D.; Sweetnam, S.; Miller, C. E.; Richter, L. J.; Kline, R. J.; Heeney, M.; McCulloch, I.; Amassian, A.; Acevedo-Feliz, D.; Knox, C.; Hansen, M. R.; Dudenko, D.; Chmelka, B. F.; Toney, M. F.; Brédas, J.-L.; McGehee, M. D. *Adv. Mater.* **2012**, *24*, 6071−6079.
(21) (a) Barnes, J. C.; Juríček, M.; Strutt, N. L.; Frasconi, M.; Sampath, S.; Giesener, M. A.; McGrier, P. L.; Bruns, C. J.; Stern, C. L.; Sarjeant, A. A.; Stoddart, J. F. *J. Am. Chem. Soc.* **2013**, *135*, 183−192. (b) Juríček, M.; Barnes, J. C.; Dale, E. J.; Liu, W.-G.; Strutt, N. L.; Bruns, C. J.; Vermeulen, N. A.; Ghooray, K. C.; Sarjeant, A. A.; Stern, C. L.; Botros, Y. Y.; Goddard, W. A., III; Stoddart, J. F. *J. Am. Chem. Soc.* **2013**, *135*, 12736−12746. (c) Barnes, J. C.; Juríček, M.; Vermeulen, N. A.; Dale, E. J.; Stoddart, J. F. *J. Org. Chem.* **2013**, *78*, 11962−11969.
(22) (a) Alers, G. B.; Golding, B.; Kortan, A. R.; Haddon, R. C.; Theil, F. A. *Science* **1991**, *257*, 511−514. (b) Wen, C.; Li, J.; Kitazawa, K.; Aida, T.; Honma, I.; Komiyama, H.; Yamada, K. *Appl. Phys. Lett.* **1992**, *61*, 2162−2163. (c) Mort, J.; Ziolo, R.; Machonkin, M.; Huffman, D. R.; Ferguson, M. I. *Chem. Phys. Lett.* **1991**, *186*, 284−286. (d) Mort, J.; Machonkin, M.; Ziolo, R.; Huffman, D. R.; Ferguson, M. I. *Appl. Phys. Lett.* **1992**, *60*, 1735−1737. (e) Xing, Y. J.; Jing, G. Y.; Xu, J.; Yu, D. P.; Liu, H. B.; Li, Y. L. *Appl. Phys. Lett.* **2005**, *87*, No. 263117.
(23) (a) Hamed, A.; Sun, Y. Y.; Tao, Y. K.; Meng, R. L.; Hor, P. H. *Phys. Rev. B* **1993**, *47*, 10873−10880. (b) Chiu, K.-C.; Su, Y.-C.; Chen, R.-S.; Lin, Y.-J.; Cheng, W.-R.; Tang, S.-J. *Jpn. J. Appl. Phys.* **2002**, *41*, 6028−6031. (c) Yang, C.-M.; Liao, J.-L.; Chiu, K.-C. *J. Appl. Phys.* **2004**, *96*, 1934−1938.
(24) (a) Frampton, M. J.; Anderson, H. L. *Angew. Chem., Int. Ed.* **2007**, *46*, 1028−1064. (b) Zhang, W.; Jin, W.; Fukushima, T.; Saeki, A.; Seki, S.; Aida, T. *Science* **2011**, *334*, 340−343. (c) Bassani, D. M. *Nature* **2011**, *480*, 326−327.
(25) Admassie, S.; Inganäs, O.; Mammo, W.; Perzon, E.; Andersson, M. R. *Synth. Met.* **2006**, *156*, 614−623.
(26) Kato, T.; Kodama, T.; Shida, T.; Nakagawa, T.; Matsui, Y.; Suzuki, S.; Shiromaru, H.; Yamauchi, K.; Achiba, Y. *Chem. Phys. Lett.* **1991**, *180*, 446−450.
(27) Aoyagi, S.; Nishibori, E.; Sawa, H.; Sugimoto, K.; Takata, M.; Miyata, Y.; Kitaura, R.; Shinohara, H.; Okada, H.; Sakai, T.; Ono, Y.; Kawachi, K.; Yokoo, K.; Ono, S.; Omote, K.; Kasama, Y.; Ishikawa, S.; Komuro, T.; Tobita, H. *Nat. Chem.* **2010**, *2*, 678−683.
(28) Iwamoto, T.; Watanabe, Y.; Takaya, H.; Haino, T.; Yasuda, N.; Yamago, S. *Chem.—Eur. J.* **2013**, *19*, 14061−14068.

DOI: 10.1021/ja512959g
J. Am. Chem. Soc. 2015, 137, 2392−2399